Astron. Astrophys. 359, 168–180 (2000)

ASTRONOMY AND ASTROPHYSICS

On the nature of the pulsation of the post-AGB star HD 56126⋆

D. Barthès[1], **A. Lèbre**[2], **D. Gillet**[3], **and N. Mauron**[2]

[1] Departament d'Astronomia i Meteorologia, Universitat de Barcelona, Avda. Diagonal 647, 08028 Barcelona, Spain
[2] Groupe de Recherche en Astronomie et Astrophysique du Languedoc–UMR 5024/ISTEEM (CNRS), Université Montpellier II, Place E. Bataillon, 34095 Montpellier Cedex 05, France
[3] Observatoire de Haute-Provence (CNRS), 04870 Saint-Michel-l'Observatoire, France

Received 6 December 1999 / Accepted 11 April 2000

Abstract. Spectroscopic and photometric observations of the variable carbon-rich post-AGB star HD 56126 are analysed in order to improve the knowledge of its pulsation and of its fundamental parameters. New high resolution spectra (R=42 000), taken as regularly as possible (every 7–9 days) from October 1995 to April 1996 at the Haute-Provence Observatory, are presented. Important profile variations of the Hα line are confirmed, and variations of Hβ are also shown for the first time. These variations can be significant over time intervals as short as ~ 7 days.

Photospheric radial velocities were derived and merged with other data from different sources to form a set of 89 values spanning ~ 8 years. We also considered a completely independent set of 87 V-band Geneva photometric measurements made over 7 years and covering approximatively the same epoch. The results of the Fourier analysis of the radial velocity and photometric series agree remarkably well: a strong main period of $P = 36.8 \pm 0.2$ days is found in both data sets. This period supersedes the value of 27 days previously found by us with much fewer data points. Weaker secondary oscillations, probably related to the irregularity of the pulsation, are also detected. There is no prominent Fourier component at $\sim 2P$ and the pulsation of HD 56126 is certainly quite different from that of RV Tauri variables.

Linear nonadiabatic analysis has been applied. It is found that the only linear radial mode that can fit the main period is the first overtone. This, together with the requirement of some driving of the pulsation and with the core mass–luminosity relation, favours the following range of fundamental parameters: $\log g$ = 0.38–0.49, $M = 0.57$–$0.63\,M_{\odot}$, $T_{\rm eff}$ = 5700–6100 K and $L = 5250$–$8160\,L_{\odot}$.

Owing to its higher temperature, the star seems more evolved than post-AGB RV Tauri's.

Hydrodynamical models are also discussed. The spectroscopic and photometric variations of the star appear to be consistent with a radial pulsation yielding shockwaves which propagate through the atmosphere and probably generate a complex, asynchronous motion of the outer hydrogen layers.

Key words: stars: atmospheres – stars: AGB and post-AGB – shock waves – line: profiles – stars: oscillations – stars: individual: HD 56126

1. Introduction

After their passage on the Asymptotic Giant Branch (AGB), intermediate and low mass stars evolve rapidly to the left of the Hertzsprung-Russel diagram, becoming progressively hotter at roughly constant luminosity. Although statistically very rare, objects in this transition phase, namely post-AGB stars, deserve detailed studies for a better understanding of the stellar evolution, particularly at the end of the AGB phase (for reviews, see e.g. van Winckel [1999] and references therein). Another interesting issue concerning these stars has been pointed out by Bond (1996, 1997): post-AGB stars of Population II with spectral type A or F are very good candidates for being new primary distance indicators, of comparable importance to the Population I Cepheids.

HD 56126 (alias SAO 96709 or IRAS 07134+1005) is one of these interesting Pop. II post-AGB stars. Quite a lot of observations have already been accumulated on this object and, in the present paper, we pursue the works of Lèbre et al. (1996, hereafter Paper I) and focus on the pulsation properties and variability of HD 56126. Very briefly, this star has the following characteristics: $l = 207°$, $b = +10°$, spectral type F5Iab, radial velocity $V_{LSR} = 72\,{\rm km\,s^{-1}}$, $T_{\rm eff}$ = 5700–7000 K, $\log g$ = 0.1–0.5. It is carbon-rich with an excess of s-elements, and also has a strong infrared excess due to a dust shell (references concerning these features can be found in Paper I). There is no convincing evidence that the star is a binary like several other post-AGB stars, but binarity cannot be definitely ruled out. Some of the parameters quoted above are not well determined and suffer from a relatively large uncertainty (as $\log g$), or they are intrinsically variable (or both). In particular, the luminosity (or the distance), and the mass of HD 56126 are not well determined, and studying the pulsation properties may help to narrow the possible range of these parameters.

Send offprint requests to: lebre@graal.univ-montp2.fr

⋆ Based on spectroscopic observations performed at the Observatoire de Haute-Provence (France) and at the European Southern Observatory (La Silla, Chile), and on photometric measurements obtained with the 70 cm Swiss Telescope at La Silla.

In Paper I, we presented the results of a first campaign devoted to the monitoring of the photospheric radial velocity (hereafter RV). Spectroscopic variations of the Hα and NaD line profiles were also investigated. These data first suggested that strong atmospheric motions were occurring, possibly with shockwave propagation. By means of Fourier and CLEAN analysis of the RV time series, we also derived several possible periods of pulsation, the main period being around 27 days. However, it was obviously necessary to increase both the number of data points and the total duration of the series. Subsequent theoretical works of Jeannin et al. (1996, 1997) have presented linear and nonlinear models of HD 56126. These models favour the first overtone as the dominant pulsation mode and reconcile the presence of relatively strong shockwaves with the small variations observed in the photometric light curve (Bogaert, 1994).

In this paper, we report on new spectroscopic observations of HD 56126. After combining our data with some from other sources, the number of RV measurements is more than 4 times larger than in Paper I, and the time span now extends to 8 years. We also consider photometric measurements, and all these data are described in Sect. 2. In Sect. 3, both time series (spectroscopic and photometric) are submitted to spectral analysis, and several periodicities are derived. The results are confronted to pulsation models in Sect. 4.

2. Description of the observations

2.1. The ELODIE spectroscopic monitoring

Spectra of HD 56126 were taken as regularly as possible from October 1995 to April 1996 at the 1.93m telescope of the Observatoire de Haute-Provence (OHP, France). The cross-dispersed ELODIE spectrograph was used (see Baranne et al. [1996] for a complete description). Briefly, this instrument provides 67 orders over a total range of about 3000 Å, from 3850 Å to 6750 Å. The detector is a thinned 1024^2 Tektronix CCD with a 24 μm pixel, and the velocity resolution is 7.1 $\mathrm{km\,s^{-1}}$ (resolving power $R = 42\,000$) as measured from Th-Ar lines.

Because the shapes and positions of the orders on the CCD are very stable, a data processing pipeline is included in the ELODIE software. We used this pipeline, which includes order extraction, bias subtraction, flat fielding with continuum lamp spectra and wavelength calibration with Th-Ar spectra. Further standard corrections were applied to correct for Earth motion and to put the wavelength scale in the "stellar rest frame" (SRF). For the latter, we adopted a center-of-mass heliocentric radial velocity of 86.1 $\mathrm{km\,s^{-1}}$, deduced from the circumstellar molecular central velocity $V_{LSR} = 72\,\mathrm{km\,s^{-1}}$ (Bujarrabal et al. 1992).

Table 1 lists the journal of these ELODIE observations with the heliocentric julian day (HJD), the gregorian date, the universal time at mid exposure ($\langle UT \rangle$), the exposure time (T), the signal-to-noise ratio at 5500 Å (s/n) and the identifier of the spectra, as used in Figs. 1 and 2. Indeed our data are labeled, throughout the text and in the figures, by means of the time (in days) elapsed since the first observation (see last column).

Table 1. Journal of the ELODIE spectroscopic observations: Heliocentric Julian day (HJD), gregorian date, Universal Time at mid exposure ($\langle UT \rangle$), exposure time (T), signal-to-noise ratio at 5500 Å (s/n) and identifier of the spectra, as used in Figs. 1 and 2.

HJD[a]	Date (mm/dd/yy)	$\langle UT \rangle$ (h:min)	T (h)	s/n	Ident
49999.670	10/09/95	04:04	1	155	10/9/95
50007.654	10/17/95	03:41	1	124	+8days
50008.629	10/18/95	03:05	1	136	+9d
50017.649	10/27/95	03:33	1	155	+18d
50024.595	11/03/95	02:14	1	77	+25d
50029.657	11/08/95	03:42	1	121	+30d
50046.594	11/25/95	02:10	1	112	+47d
50053.612	12/01/95	02:34	1.5	143	+54d
50061.630	12/10/95	03:52	1	105	+62d
50070.583	12/19/95	01:52	1	82	+71d
50085.618	01/02/96	02:42	1	84	+86d
50086.656	01/04/96	03:36	2	108	+87d
50102.485	01/19/96	22:22	1	140	+103d
50154.394	03/11/96	21:24	1	93	+155d
50179.317	04/05/96	19:36	1	117	+180d
50186.324	04/12/96	19:47	1	124	+187d

[a] Heliocentric Julian Day: + 2 400 000.0000

2.2. Complementary spectroscopic observations

Until mid-1998, we also had the opportunity, from time to time, to access other instruments: the 1.52m telescope at the OHP, equiped with the AURELIE spectrometer (observational set-up already described in Paper I) and the CAT/CES at ESO La Silla (on Hα, the resolving power is 60 000, and the spectral dispersion is 1.98 Å/mm – see Kaper & Pasquini [1996]). These additional Hα observations, listed in Table 2, were very welcome to ensure a good time resolution of our spectroscopic monitoring.

2.3. The Hydrogen Balmer lines

Fig. 1 shows the Hα profiles coming from the ELODIE monitoring supplemented by the first five AURELIE spectra. As already noted in Paper I, the Hα line is strongly variable and always exhibits one or two emission wings. Note also the broad, smooth absorption wings on both sides of the variable core (discussed in Paper I). A sequence of Hβ profiles is shown for the first time in Fig. 2, and profile variations are clearly detected. This line always exhibits a broad absorption profile with a core like Hα; at some dates, however, weak emission shoulders emerge on the blue or the red edge of the core. This is particularly clear at dates + 18 d, +180 d and +187 d. It is worth noting that these emission shoulders in Hβ exactly coincide with the emerging of important emission features in Hα.

We have carefully examined these two Balmer lines to search for typical timescales, or variation cycles. One can see a slow but progressive variation of the profiles over the first 30 days. There is no sign of periodicity of about 27 days which was the main period found in Paper I. Searching for couples of very similar profiles, one finds intervals of about 100–110 days

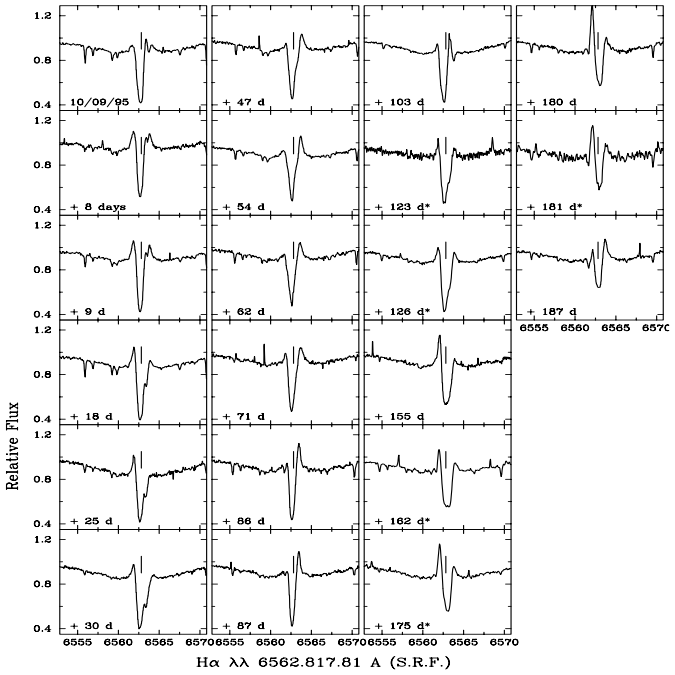

Fig. 1. Part of spectroscopic observations of the Hα line region. The Hα wavelength in the stellar rest frame is indicated by vertical ticks. The date of each observation is given in days elapsed after the first spectrum. A date with an asterisk ($*$) indicates an AURELIE spectrum. These Hα plots constitute the most homogeneous and continuous observational series, among all data listed in Tables 1 and 2.

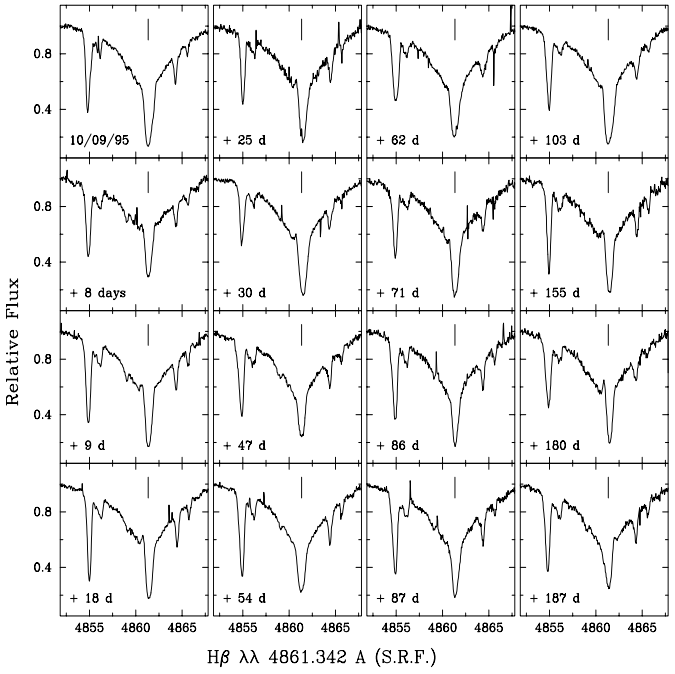

Fig. 2. Spectra of the Hβ line. The Hβ wavelength in the stellar rest frame is indicated by vertical ticks. Emission is clearly seen at dates +18 d, +180 d and +187 d. A few very narrow spikes are due to cosmic rays.

Table 2. Supplementary spectroscopic observations of the Hα line: last column indicates the instrumental origin of the spectrum: AURELIE at 1.52m telescope (OHP); CES at 1.4m CAT (ESO).

HJD[a]	Date (mm/dd/yy)	$\langle UT \rangle$ (h:min)	T (h)	Ident	from[b]
122.549	02/09/96	01:04	2.5	+123d*	A
125.489	02/11/96	23:37	2.5	+126d*	A
161.374	03/18/96	20:56	3.5	+162d*	A
174.342	03/31/96	20:12	2.2	+175d*	A
181.328	04/07/96	19:53	2.5	+181d*	A
766.811	11/14/97	07:24	1.3		C
767.825	11/15/97	07:43	1.5		C
768.823	11/16/97	07:40	1.5		C
772.754	11/20/97	06:01	1.4		C
845.433	01/31/98	22:16	2.0		A
854.462	02/09/98	22:59	2.0		A
857.460	02/12/98	22:56	2.0		A
858.457	02/13/98	22:51	2.0		A
859.450	02/14/98	22:41	2.0		A
860.463	02/15/98	23:00	2.0		A
861.463	02/16/98	23:01	2.0		A
862.423	02/17/98	22:03	2.0		A
902.338	03/29/98	20:05	2.0		A

[a] Heliocentric Julian Day: + 2 450 000.0000
[b] A: AURELIE; C: CES

(from spectra 10/09/95 and +103d; spectra +18d and +155d; spectra +30d and +180d; spectra +47d and +187d). However, since the sampling during the ELODIE monitoring is irregular, we may have missed important profile variations occurring between two consecutive observations. This is actually obvious from our last two observations (+180d and +187d), which show drastic changes of the Hα and Hβ profiles within only 7 days. Concluding, the variations of Hα and Hβ shown in Figs. 1 and 2 do not exhibit any obvious pseudo-periodicity resembling or related to the ones found in the photospheric radial velocity (see Paper I, and next section). The mechanism responsible for these line variations is probably very complicated (see Sect. 4).

2.4. Photospheric radial velocity data

As already mentioned in Paper I, the Ba II λ 5853.688 Å and C I λ 6587.622 Å lines are two interesting strong features observed in the spectra of HD 56126. Indeed, these lines are not blended with any other spectral feature and their profiles are always fairly symmetric. Their radial velocities are also quite well synchronized (Ba II and C I RV measurements made in the same night generally agree within 1.5 $\mathrm{km\,s^{-1}}$, see Paper I). This indicates that the atmospheric (photospheric) layers where these lines form have the same dynamics.

As a consequence and for consistency with Paper I, we always adopted these two lines for measuring the RV variations. A number of new RV values were derived in this way from spectra listed in Tables 1 and 2. The typical accuracy is 0.8 $\mathrm{km\,s^{-1}}$ for ELODIE and CES measurements, and 1.0 $\mathrm{km\,s^{-1}}$ for AURELIE data. In addition, Dr. E. Bakker (private communication)

Table 3. Supplementary spectroscopic observations (kindly provided by E. Bakker). Columns 1 and 2 present the Julian and Gregorian dates. Last column indicates the instrumental origin of the observation. Note that the observation presented in Klochkova (1995) is included too.

HJD[a]	Date (mm/dd/yy)	from[b]
47899.821	01/08/90	P
48677.406	02/24/92	WHT
49000.385	01/12/93	K
49030.9	02/12/93	McD
49333.7	12/12/93	McD
49335.7	12/14/93	McD
49337.6	12/16/93	McD
49338.8	12/17/93	McD
49342.481	12/20/93	WHT
49371.6	01/19/94	McD
49371.7	01/19/94	McD
49410.504	02/27/94	WHT
49790.704	03/14/95	C
49826.575	04/19/95	C
50059.912	12/08/95	C
50098.858	01/16/96	C

[a] Heliocentric Julian Day: + 2 400 000.0000
[b] C: CES/CAT; P: Palomar; McD: McDonald 2.7m telescope; WHT: WHT/UES; K: Russian 6m telescope (from Klochkova, 1995)

kindly gave us 14 RV measurements which nicely fill a gap between our 2 OHP monitorings. These supplementary spectroscopic observations are listed in Table 3. All these spectra come from high resolution optical and near-infrared spectra collected by several observers using different instruments (Palomar, McDonald, WHT/UES, CES). They are thus inhomogeneous, but the uncertainty of each point is probably about 1–2 $\mathrm{km\,s^{-1}}$.

The resulting set of heliocentric RV data is shown in Fig. 3a, and listed in Table 4. It covers a time span of about 8 years, from JD 2 447 899 to 2 450 902. As mentioned above, the stellar rest frame velocity, derived from millimetric CO emission, equals $86.1 \pm 1.3\,\mathrm{km\,s^{-1}}$ and is indicated by a horizontal dashed line in Fig. 3. It clearly differs from the mean ($87.68 \pm 0.31\,\mathrm{km\,s^{-1}}$), the median ($87.57 \pm 0.07\,\mathrm{km\,s^{-1}}$) and the less-biased phase-averaged mean[1] ($87.96 \pm 0.61\,\mathrm{km\,s^{-1}}$) of our RV data. These differences are little significant, with confidence levels of respectively 57, 54 and 63% according to Student's test. However, one also observes a weak trend over the whole time span ($+5.10\,10^{-4} \pm 3.4\,10^{-4}\,\mathrm{km\,s^{-1}}$ per day), with a confidence level of 63%. It cannot be due to the instruments or the data processing, since the data coming from different sources are intermingled. If this coincidence were fortuitous, its probability would be about 15%. This strongly suggests that some deterministic phenomenon is operating – for example an oscillation due to a companion orbiting with a period > 16 years. More data are needed to clarify this point.

[1] obtained by folding the data set on a cycle of 36.7 days (see Sect. 3), divided in 10 phase bins

Table 4. Heliocentric radial velocity (RV) measurements. Data already presented in Table 4 of Paper I are not reported again. The typical uncertainty on RV is 0.8 $\mathrm{km\,s^{-1}}$ for ELODIE and CES measurements, and 1.0 $\mathrm{km\,s^{-1}}$ for AURELIE data. Data provided by E. Bakker (inhomogeneous data set) present an uncertainty of about 1–2 $\mathrm{km\,s^{-1}}$

HJD[a]	RV ($\mathrm{km\,s^{-1}}$)	HJD	RV ($\mathrm{km\,s^{-1}}$)
47899.821	85.50	50085.618	87.81
48677.406	82.30	50086.656	88.14
49000.385	90.8	50098.858	90.87
49030.9	85.5	50102.485	89.73
49333.7	85.8	50122.549	88.51
49335.7	84.8	50125.489	87.51
49337.6	84.8	50154.394	90.50
49338.8	85.0	50161.374	86.86
49342.481	87.00	50174.342	87.88
49371.6	85.2	50179.317	83.87
49371.7	86.9	50181.328	80.13
49410.504	84.00	50186.324	85.41
49790.704	86.89	50766.811	87.97
49826.575	93.30	50767.825	87.73
49999.670	83.25	50768.823	87.51
50007.654	86.74	50772.754	83.95
50008.629	87.20	50845.433	86.96
50017.649	93.49	50854.462	89.47
50024.595	91.99	50857.460	89.56
50029.657	86.19	50858.457	90.27
50046.594	88.68	50859.450	90.64
50053.612	89.71	50860.463	92.00
50059.912	89.21	50861.463	92.87
50061.630	86.19	50862.423	92.33
50070.583	88.27	50902.338	94.33

[a] Heliocentric Julian Day: + 2 400 000.0000

2.5. Photometric data

A total of 87 V photometric measurements of HD 56126 were kindly provided by Drs. C. Waelkens and G. Burki. They are listed in Table 5 and plotted in Fig. 4. They were collected between HJD 2447489.8 and 2450112.6 with the 70 cm Swiss telescope at La Silla Observatory. The noise level is low ($\sigma = 0.005$ mag), to be compared to the star variations of about 0.15 mag. A detail of the V light curve of HD 56126 is shown in Fig. 4a and b and was published for the first time by Bogaert (1994). This photometric data set is another high quality database for searching for periods. It spans about 7 years, overlapping the RV series for about 4 years.

3. Period searching

In order to determine the pulsation period(s) of the star, we have performed a spectral analysis of the 89 velocity data shown in Fig. 3, whatever their origin. Spectral analysis has also been performed on the 87 V photometric observations (see Fig. 4). Concerning the RV series, we have decided to neglect the inconvenience of using heterogeneous spectral lines and instruments, because the main problems to solve are the perturbing

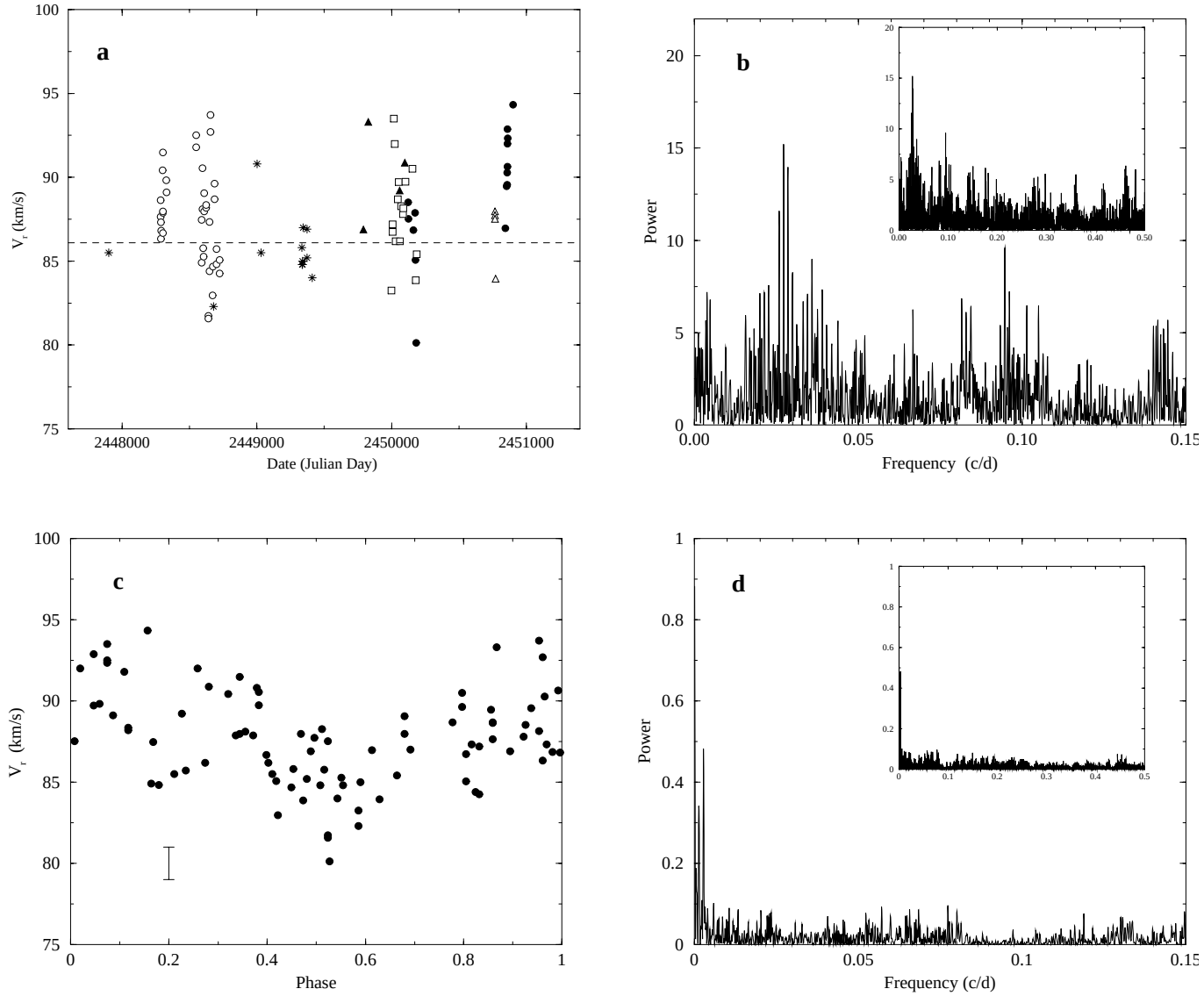

Fig. 3. a Photospheric radial velocities in HD56126. The horizontal dashed line indicates the central radial velocity of molecular circumstellar profiles, $V_{helio} = 86.1 \pm 1.3\,\mathrm{km\,s^{-1}}$. The different contributions to the data set are as follows: circles stand for AURELIE observations (filled: data described in Table 2; open: data described in Paper I); open squares stand for ELODIE observations (described in Table 1); stars stand for data kindly provided by E. Bakker (private communication); triangles stand for CAT/CES observations (filled symbol for data provided by E. Bakker). **b** Lomb-Scargle periodogram. **c** Folded velocity curve, assuming period 36.7 d. Typical error bars ($\pm 1\,\mathrm{km\,s^{-1}}$) are shown. **d** Spectral window.

effects of the unequal time-spacing and limited duration of the data in the presence of noise. This choice is likely to affect the computed amplitudes, rather than the periods. Moreover, we take $\sigma = 1\,\mathrm{km\,s^{-1}}$ as a conservative estimate of the observational noise (in fact, $\sigma \simeq 0.8\,\mathrm{km\,s^{-1}}$ for the data coming from ELODIE, and less for those from the ESO).

The raw power spectra of these data have been computed by means of the Lomb-Scargle periodogram (Scargle 1982, Press et al. 1992), which is known to be less sensitive to noise and irregular data spacing than the discrete Fourier transform. The obtained spectra (see Figs. 3b and 4c) are complicated, but this is not due to the noise, which is so low (respectively 0.52 and 0.13 at a confidence level of 99.3%) that it cannot be displayed in these figures. Both spectra exhibit a prominent, split feature (i.e. a bundle of large-amplitude peaks) around frequencies 2.50–$2.90\,10^{-2}$ c/d, i.e. period 37 ± 3 days. The largest peak is the same, at frequency $2.715 \pm 0.008\,10^{-2}$ c/d (hence a period of about 36.8 day).

The deconvolution method used in the present paper is basically the CLEAN algorithm, simply adapted to our purpose. In every implementation, the iteration gets stopped as soon as no frequency liable to be selected exceeds the noise level (with 99.3% confidence), computed in the same way as in Barthès et al. (1996). The standard version of the CLEAN method (i.e.,

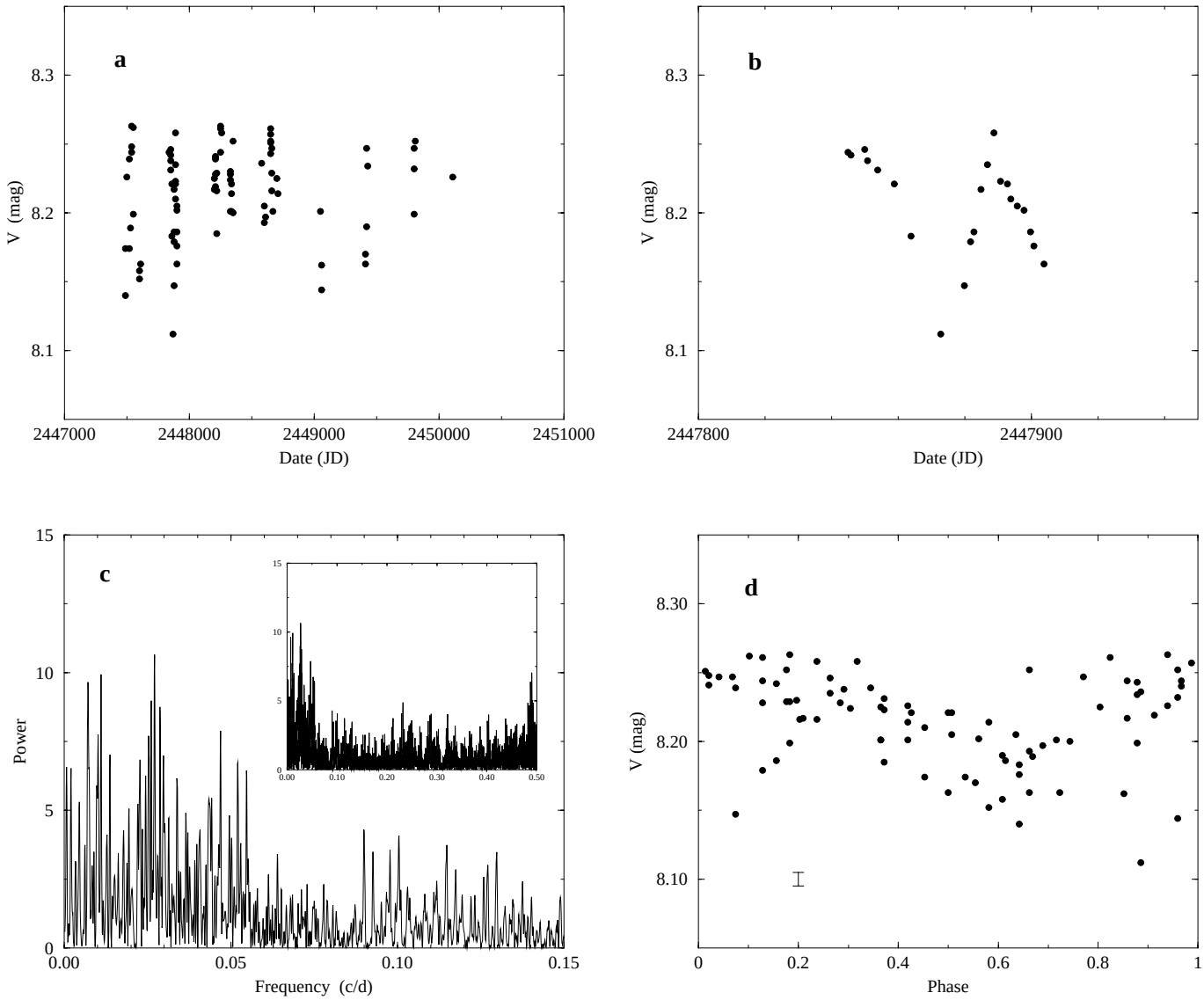

Fig. 4. Photometric data set (**a** full time span; **b** detail), its Lomb-Scargle periodogram **c** and the folded lightcurve, assuming period 37 d **d**. Typical error bars (± 0.005 mag) are shown.

simply selecting, at every iteration, the largest-amplitude peak, and subtracting a small part [$\leq$ 10%] of its overall contribution) either diverges or converges towards unrealistic solutions in which the low-frequency power (which is most probably real) appears randomly redistributed towards high frequencies. We have overcome this problem by enforcing additional constraints, in order to prevent the algorithm from "hesitating" between equivalent solutions.

Indeed, considering the aspect of the lightcurve (two relatively well-sampled pseudocycles, shown in Fig. 4b, suggest a nearly periodic pulsation) and the fact that the periodogram gets its maximum power at the same frequency for two completely independent data sets, it seems reasonable to assume that this component does correspond to the mean timescale of the main pulsation. Then, its close neighbours would be combined effects of data sampling and signal fluctuations. We thus start the CLEAN iteration from this component, using a relatively large gain factor ($\eta > 0.7$), then we release this strong *a priori* constraint by quickly reducing η (70 or 80% less at every next iteration) down to 0.05. For maximum security, it is wise to also try the other possibilities and to select the "cleanest" solution, i.e. the one that has the largest main-signal-to-background ratio.

Finally, for further discussion, we have selected, in the cleaned spectra, the largest-amplitude component and also the few other most-significant peaks, according to the following criteria:

1. frequency lower than ten times the "average" Nyquist frequency, which is $\nu_{\overline{N}} = 1/2\overline{\delta t}$, with $\overline{\delta t}$ being the average time spacing of the data ($\nu_{\overline{N}} = 0.015$ c/d for the radial velocity and 0.017 for the photometric data);
2. power exceeding the estimated noise at the 99% confidence level;

Table 5. Photometric measurements (V magnitude) obtained with the 70 cm Swiss Telescope at La Silla Observatory (kindly provided by Drs. C. Waelkens and G. Burki). The typical uncertainty on V magnitude is about 0.005 mag.

HJD[a]	Date (mm/dd/yy)	V	HJD	Date (mm/dd/yy)	V
47489.805	11/24/88	8.174	48218.837	11/23/90	8.216
47493.790	11/28/88	8.140	48223.808	11/28/90	8.185
47504.778	12/09/88	8.226	48245.769	12/20/90	8.244
47519.780	12/24/88	8.239	48251.748	12/26/90	8.261
47523.778	12/28/88	8.174	48253.739	12/28/90	8.263
47531.691	01/05/89	8.189	48255.731	12/30/90	8.258
47538.770	01/12/89	8.244	48328.352	03/12/91	8.230
47541.712	01/15/89	8.263	48331.462	03/15/91	8.228
47544.734	01/18/89	8.248	48332.339	03/16/91	8.224
47547.737	01/21/89	8.262	48334.543	03/19/91	8.201
47550.729	01/24/89	8.199	48336.547	03/21/91	8.201
47602.578	03/17/89	8.152	48339.540	03/24/91	8.221
47603.565	03/18/89	8.158	48342.516	03/27/91	8.214
47605.538	03/20/89	8.163	48345.568	03/30/91	8.252
47844.846	11/14/89	8.244	48348.543	04/02/91	8.200
47845.784	11/15/89	8.242	48575.671	11/15/91	8.236
47849.832	11/19/89	8.246	48603.591	12/13/91	8.205
47850.764	11/20/89	8.238	48604.569	12/14/91	8.193
47853.770	11/23/89	8.231	48605.568	12/15/91	8.197
47858.772	11/28/89	8.221	48647.493	01/25/92	8.261
47863.754	12/03/89	8.183	48649.443	01/27/92	8.243
47872.728	12/12/89	8.112	48652.465	01/30/92	8.252
47879.750	12/19/89	8.147	48653.437	01/31/92	8.257
47881.689	12/21/89	8.179	48654.468	02/01/92	8.251
47882.716	12/22/89	8.186	48655.467	02/02/92	8.247
47884.760	12/24/89	8.217	48660.453	02/07/92	8.229
47886.729	12/26/89	8.235	48661.448	02/08/92	8.216
47888.685	12/28/89	8.258	48667.386	02/14/92	8.201
47890.673	12/30/89	8.223	48704.524	03/23/92	8.225
47892.687	01/01/90	8.221	48706.535	03/25/92	8.214
47893.774	01/02/90	8.210	49050.542	03/04/93	8.201
47895.689	01/04/90	8.205	49055.543	03/09/93	8.162
47897.702	01/06/90	8.202	49059.537	03/13/93	8.144
47899.716	01/08/90	8.186	49412.582	03/01/94	8.163
47900.674	01/09/90	8.176	49414.558	03/03/94	8.170
47903.673	01/12/90	8.163	49416.594	03/05/94	8.190
48202.693	11/07/90	8.225	49422.607	03/11/94	8.247
48204.666	11/09/90	8.217	49426.546	03/15/94	8.234
48206.860	11/11/90	8.219	49796.537	03/20/95	8.199
48208.752	11/13/90	8.240	49799.536	03/23/95	8.232
48210.849	11/15/90	8.241	49803.540	03/27/95	8.247
48212.810	11/17/90	8.239	49807.549	03/31/95	8.252
48214.834	11/19/90	8.228	50112.608	01/30/96	8.226
48216.824	11/21/90	8.229			

[a] Heliocentric Julian Day: + 2 400 000.0000

3. amplitude larger than 30% of the one of the main component;
4. the peak also appears, and matches the 2nd and 3rd criteria, in the CLEAN spectrum of the residual obtained by subtracting the main component from the data.

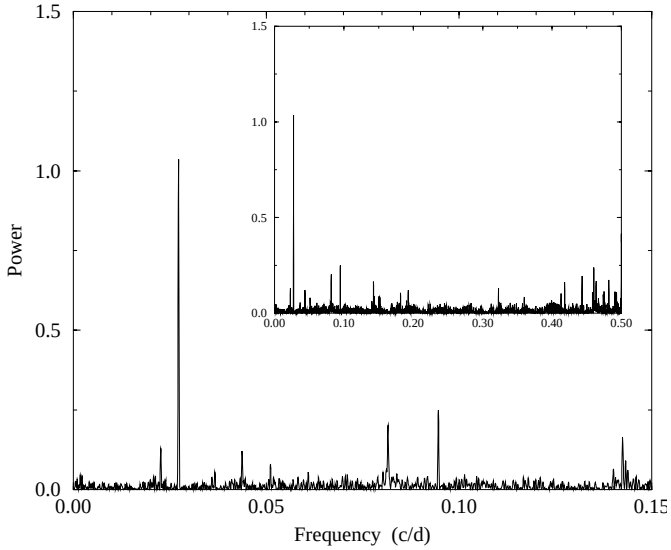

Fig. 5. CLEAN spectrum of the velocity data.

As a last step, the frequencies, semi-amplitudes and phases of these selected components were adjusted by means of a non-linear least-squares fit.

We must warn the reader that the definition of the power is not the same in the Lomb-Scargle periodogram and in the Fourier or CLEAN spectrum. The latter is simply one fourth of the squared semi-amplitude at the considered frequency, while the former includes a factor depending on the variance of the data. Hence the different scaling of the spectra shown in Figs. 3 and 4 on the one hand, and 5 & 6 on the other.

3.1. Photospheric radial velocities

A very clean power spectrum is obtained, as shown in Fig. 5, where the noise level (99.3% CL) is only about $0.056\,\mathrm{km}^2/\mathrm{s}^2$ (semi-amplitude $0.47\,\mathrm{km\,s}^{-1}$). No better solution is found when starting from any other component of the main feature of the raw spectrum or from its second largest feature (around 0.0946 c/d).

The main period is 36.7 days. Apart from this component, which frequency is hereafter called ν_a, four peaks are found most significant according to the above-mentioned criteria. Their frequencies are 0.0226 (ν_b), 0.0816 ($3\nu_a$), 0.0947 (ν_c) and 0.1042 (ν_d). They are listed in Table 6. It must however be mentioned that, if a few data points are removed, the results may slightly differ: the peak at 0.0226 c/d often becomes unsignificant and is replaced by 0.0367 c/d which, in the cleaned spectrum of the whole data set, does not match our 3rd criterion, though it matches the 1st, 2nd and 4th. This component is mentioned between brackets and called [ν_e] in Table 6.

The nonlinear fit changes the frequencies by less than 0.3% (0.1% for the main component), which is reassuring, and gives a residual $\sigma = 1.4\,\mathrm{km\,s}^{-1}$, just a bit larger than the error bars of the data. On the other hand, a nonlinear fit of only the main component and its third harmonic gives a main amplitude of

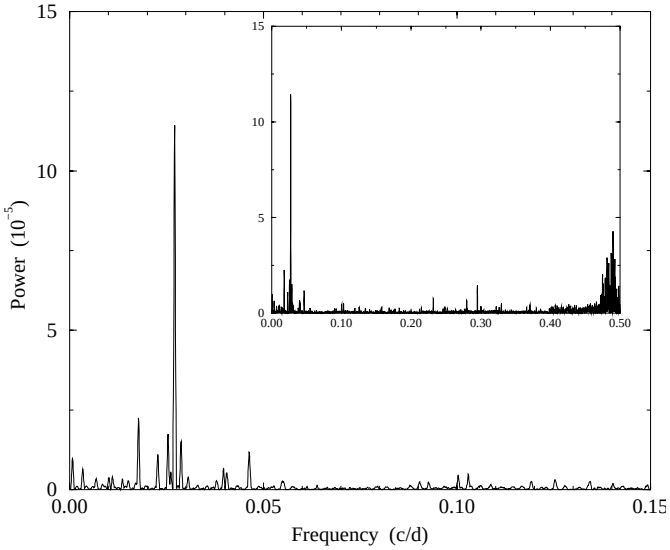

Fig. 6. CLEAN spectrum of the photometric data.

$2.4\,\mathrm{km\,s^{-1}}$ and a residual of $\sigma = 2.2\,\mathrm{km\,s^{-1}}$, which is about twice the expected value. The corresponding folded velocity curve is shown in Fig. 3c: an oscillation with about one third of the main period is visible, together with irregularities exceeding the noise level. Confrontation with the spectral window has shown that the other selected components do not correspond to any alias of the main periodicity. Summarizing, the pulsation is certainly not single-periodic and the secondary components are not merely due to a failure of the deconvolution.

3.2. Photometric data

Deconvolution of the spectrum of the magnitude variations appears a bit more difficult. The CLEAN iteration diverges, whatever the gain and the starting point. We thus decided to slightly restrict the domain in which CLEAN components may be selected, by setting a cut-off frequency at 0.4 c/d (instead of 0.5). Then, we proceeded in the same way as in the preceding subsection.

The cleaned power spectrum is shown in Fig. 6, where the noise level (99.3% CL) is about $1.4\,10^{-6}\,\mathrm{mag}^2$ (semi-amplitude 2.4 mmag). Starting from any other component of the main feature yields a smaller main-signal-to-background ratio.

The main period is 36.9 days, in very good agreement with the result from RV data. Apart from this main component ν_a, five other most-significant peaks are found and called ν_x, ν_y, $\nu_z = \nu_x + \nu_y$, ν_b and $2\nu_a - \nu_y$ (see Table 6).

Here too, the nonlinear fit changes the frequencies by less than 0.3% (the main period shifts to 37.0 d). The residual is $\sigma = 0.017$, about 3 times the error bars of the data. This means that a significant part of the signal power is still spread over the whole spectrum, especially above the cut-off frequency (see Fig. 6). A fit of only the main component gives amplitude 23 mmag and a residual $\sigma = 29$ mmag (28 if its second and third harmonics are also included), i.e. 6 times the data errors. The corresponding folded lightcurve is shown in Fig. 4d and appears noisy above the noise level. The main periodicity is thus certainly not the only component. Moreover, none of the selected components corresponds to any alias of the main periodicity. They are thus probably real.

3.3. Hydrogen lines

As mentioned in Sect. 2, the sequences of Hα and Hβ profiles shown in Fig. 1 and 2 do not exhibit any obvious periodicity of the order of the ones found in the photospheric radial velocity. The complexity of the line profiles and of the underlying physical phenomena makes it very difficult to select a simple characteristic that would permit us to follow throughout the time one physical variable of the concerned atmospheric layers (e.g. the velocity). Nevertheless, we have computed, as a first guess, the Lomb-Scargle periodogram and the classical CLEAN spectrum of the varying position of the intensity minimum in the Hα line (for all the data listed in Tables 1 and 2 of this paper and in Paper I, extending over 2633 days). A single, very significant periodicity at freq. $3.68\,10^{-3}$ c/d (272 days) is obtained, with an equivalent velocity semi-amplitude of $1.3\,\mathrm{km\,s^{-1}}$ (which does not necessarily correspond to a real velocity oscillation!). It does not correspond to any significant peak of the photospheric velocity spectrum. Moreover, no secondary periodicity is observed.

3.4. Discussion on the period search results

It was said above that a nonlinear fit of only the main component (even with harmonics) yields a large residual. Furthermore, if we reconstruct a model light- or velocity curve sampled exactly like the data, then the periodogram is very different from the real one: it includes only a few significant aliases, and their amplitude ratios with respect to the model periodicities are much smaller than those observed in the real spectra. This holds too if the model curves are made from the six most-significant Fourier components. All this strongly suggests that the pulsation of HD 56126 is not merely periodic or quasiperiodic, and that its basic "periodicities" are fluctuating (chaotic signal), generating wide features instead of Dirac peaks and thus, after convolution with the spectral window, bundles of large-amplitude peaks. As the CLEAN method is based on the assumption that the real spectrum is a set of Dirac peaks, it is not surprising that we got implementation difficulties and had to enforce additional constraints.

The frequencies, periods and (semi-)amplitudes of the most-significant components of the two deconvolved spectra are listed in Table 6. The uncertainty of the frequencies or periods is difficult to estimate. It is influenced, not only by the irregular data spacing, but also by the signal fluctuations. *A priori*, it may be larger than the ideal resolution interval (about $\pm 3.6\,10^{-4}$ c/d), but must be smaller than the half-width of the main feature (about $\pm 2\,10^{-3}$ c/d). However, for the main component, additional information is provided by the very small frequency shift observed between the two totally independent data sets: the uncertainty should be about 0.3%, and thus the main period

of the star is conservatively 36.8 ± 0.2 days. Concerning the other peaks, the uncertainty might be larger, since the quality of the deconvolution depends on the accuracy of the starting frequency.

Among the other most-significant components found in the velocity spectrum, none is detected in the cleaned spectrum of the lightcurve as reliably as ν_a, which is the only strong, common feature. In other terms, at least within the frame of our data set, the atmosphere of HD 56126 appears to undergo a basically periodic motion with a period of 36.8 days.

Nevertheless, the component ν_b, too, is common to both spectra, although it is relatively unstable. Moreover, $\nu_x + \nu_y$ corresponds to $\nu_d - \nu_c$. The components $3\nu_a$ and ν_d, absent from the lightcurve spectrum, appear peculiarly stable when part of the RV data are removed (see, e.g., Paper I). All these facts supplement the significance criteria given above, so confirming the presence of low-amplitude secondary oscillations in both variability curves.

No trace of the single frequency detected in the Hα line is found in the photospheric velocity spectrum. In the lightcurve spectrum, only the width of the main feature (main peak and neighbours) might be related to it.

Another striking fact is the absence of any significant feature around half the main frequency. The pulsation of HD 56126, with its single strong periodicity, is thus very different from the one of RV Tauri stars, characterized by a 2:1 resonance (see next section).

In Paper I, based on 21 AURELIE RV determinations spread over only 450 days, we gave 27.3 days as the probable main pulsation period, because it had the largest amplitude. Obviously, our new results are different. As said above, the period 27.3 d (ν_e) is now marginally significant and its amplitude appears very sensitive to the number of data. A folded velocity curve based on this period looks totally noisy. The period 36.8 d was not explicitly mentioned in Paper I but, in fact, it appeared as a secondary peak in the wide feature found at 32.9 days (see Fig. 9 of Paper I). This does not necessarily mean that the 27.3 d period (nor even the new one!) was an artefact due to bad deconvolution, or that the main pulsation mode has changed since the first observations. A chaotic pulsation can explain everything as well. Indeed, in this case, any Fourier spectrum obtained from a data sample is the convolution of the spectral window by a random sample of the actual, continuous spectrum of the pulsation. Then, the solution found by the CLEAN algorithm must *not* be considered as *the* solution: it is *one* model among an infinity, valid only at some epoch of the star history and for a given sampling. If some data points are removed, or if another epoch is investigated, or if other reasonable constraints are applied, it is nothing but natural that some Fourier components become less – and some others more – significant. In particular, the largest-amplitude frequency may differ a lot from the actual value, with an increasing probability as the data number and time span decrease, especially if the data sampling is as odd as in Paper I ("average" Nyquist frequency 0.0233 c/d, i.e. 43 d !). In other terms, we are confident that the period 36.8 days is much more reliable than the previous 27.3 d, and that most of the 6 Fourier components found in the velocity curve or in the lightcurve are real, but this solution is certainly neither complete nor perfectly stable. It is simply a better insight into the actual behaviour of the star.

4. Nature of the pulsation

4.1. Linear analysis

As shown in the previous section, consistently with dynamical models (see below), the pulsation has a definite main timescale, but it is not merely periodic. Hoping to understand the frequency components listed in Table 6, we have computed the radial modes of a series of models by using a linear nonadiabatic (LNA) code, described in Tuchman et al. (1978, 1993), together with recent opacity tables (OPAL92). The reflecting outer boundary condition of Cox & Giuli (1968) is assumed. Convection is treated according to the mixing-length formalism of Cox & Giuli (1968), with instantaneous adjustment to the pulsation. The adopted mixing-length parameter is $\lambda = 1.6$, since this value has been found convenient for the Sun and the RGB with these opacity tables (Castellani et al. 1992, Claret & Giménez 1992, Schaller et al. 1992, Bressan et al. 1993).

Concerning the stellar parameters to be adopted, various estimates of the effective temperature and the gravity have been previously published. Parthasarathy et al. (1992) gave $T_{\rm eff}$ = 6500 K and $\log g$ = 0.5 . Klochkova (1995) found 7000 K and $\log g$ = 0.1. In Paper I we found $T_{\rm eff} = 5750 \pm 250$ K and $\log g$ = 0.5 . On these grounds, we decided to explore the following range of stellar parameters: M = 0.4–0.7 $M_\odot$ (larger masses are unlikely for a Pop. II Post-AGB star) and $T_{\rm eff}$ = 5000–7000 K. The luminosity was derived from the assumed gravity. The models were computed for metallicity Z = 0.001, a value which is normal for a Pop. II star, and not far from [Fe/H] = -1, given by Parthasarathy et al. (1992) and Klochkova (1995). Varying Z by a factor 2 shifts the period of each mode by about 1% only.

The first result of these calculations is that the parameters published by Klochkova (1995) are far beyond the limit of dynamical instability. At such a high temperature, a gravity $\log g \geq 0.5$ would be required so as to stabilize the star.

Adopting $0.2 \leq \log g \leq 0.5$, all radial modes are usually found linearly stable. There are however windows of pulsational instability for the fundamental mode (always below 5500 K) and for the second and higher overtones, in a temperature domain that depends on the gravity and mass as shown in Fig. 7. At a given gravity and mass, the period of each mode does not evolve straightforwardly with the temperature: it may oscillate within 5% of a mean value. Since the fundamental mode is always longer than 47 days, and the second overtone shorter than 28 d, the first overtone is the only radial mode that may match the main period, 36.8 days, as shown in Fig. 7. This happens for gravities ranging from 0.3 to 0.5. Unfortunately, this mode is always linearly damped. Its driving, if it occurs, must originate from its nonlinear coupling with linearly unstable higher-order modes. This restricts the range of permitted parameters to $T_{\rm eff}$ =5600–6100 K and $L = 4600$–$8500 L_\odot$.

Table 6. Frequencies, periods and semi-amplitudes (according to CLEAN and after non-linear fit) of the most significant Fourier components of the velocity- and light-curves, compared to a typical linear nonadiabatic model (frequencies, periods and growth-rates per period), with parameters 0.6 $M_\odot$, 5903 K and 6655 $L_\odot$.

Radial velocity				Brightness				Model		
ident	ν $[10^{-2}\,\mathrm{c/d}]$	P [d]	A [km s^{-1}]	ident	ν $[10^{-2}\,\mathrm{c/d}]$	P [d]	A [mmag]	ν $[10^{-2}\,\mathrm{c/d}]$	P [d]	η
								1.31	76.3	−0.16
				ν_x	1.78	56.2	9–18			
ν_b	2.26	44.2	0.7–1.1	ν_b	2.27	44.0	6–6			
				$2\nu_a - \nu_y$	2.54	39.4	8–15			
ν_a	**2.72**	**36.7**	**2.0–2.7**	ν_a	**2.71**	**36.9**	**21–20**	**2.71**	**36.8**	−0.25
				ν_y	2.88	34.8	8–17			
$[\nu_e]$	[3.67]	27.3	0.5–1.2							
				$\nu_x + \nu_y$	4.64	21.6	7–14			
								5.77	17.3	−0.00
								7.45	13.4	−0.03
$3\nu_a$	8.16	12.2	0.9–1.0							
ν_c	9.47	10.6	1.0–1.5							
								10.67	9.4	+0.04
								12.40	8.1	+0.11
								12.77	7.8	+1.98
ν_d	14.25	7.0	0.8–0.6							

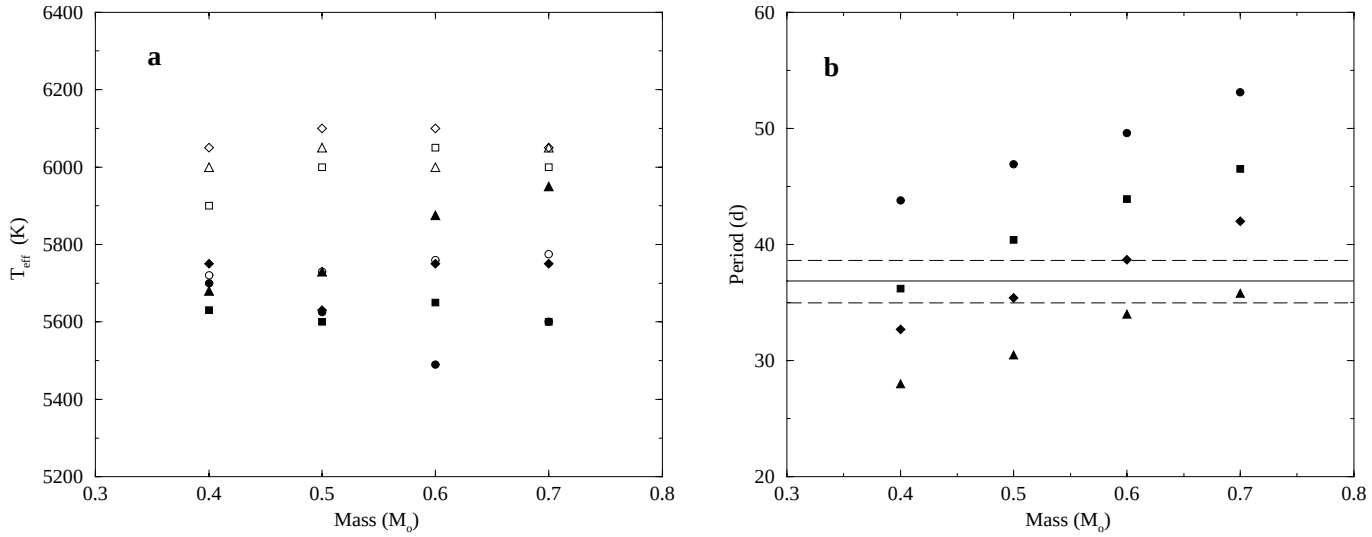

Fig. 7. a Minimum (filled symbols) and maximum (open symbols) temperatures of the overtone pulsational instability domain, as a function of the mass and for gravity $\log g$ = 0.2 (circles), 0.3 (squares), 0.4 (diamonds) and 0.5 (triangles). **b** Temperature-averaged period of the first overtone as a function of mass and gravity. The horizontal lines denote the observed period $\pm 5\%$ (amplitude of the period fluctuation of the theoretical mode according to the temperature).

For a post-AGB star, the fundamental parameters are further constrained by the AGB core mass-luminosity relation. We have adopted the one of Boothroyd & Sackmann (1988), which takes metallicity into account and holds for core masses (thus post-AGB total masses) lower than 0.7 $M_\odot$. It is also virtually insensitive to the mixing-length parameter. Then, allowing for a possible 5% fluctuation of the first overtone period, the range of fundamental parameters reduces to: $\log g$ = 0.38–0.49, M = 0.57–0.63 $M_\odot$, $T_{\rm eff}$ = 5700–6100 K and L = 5250–8160 $L_\odot$. Although the nonlinear periods and instability domain probably differ from these LNA results, this range of fundamental stellar parameters is our best approximation to the actual values, if the star is indeed pulsating on the first overtone.

As an example, one of these models (0.6 $M_\odot$, 5903 K, 6655 $L_\odot$, i.e. $\log g$ = 0.43) is given in Table 6. Its fifth and sixth overtones are significantly excited (note however that, in the real star, the energy leakage due to the formation of shocks, i.e. the imperfect reflection at the outer boundary, should decrease these growth rates).

It would be vain to seek for a linear model that would precisely account for the most-significant Fourier components, for Aikawa (1991) has shown that the nonlinear periods of post-AGB models may differ from the linear ones by as far as 10%. It is possible that the Fourier components ν_c and ν_d correspond to, e.g., the fourth and sixth overtones, if the star is indeed pulsating on the first overtone. However it remains difficult to explain the other components, especially those of the brightness variation.

LNA analysis puts also lights on the issue whether a mode switch has occured since Paper I. Indeed, it is only for $\log g \simeq 0.2$, $M \simeq 0.7\,M_\odot$, $T_{\rm eff} \simeq 5800\,{\rm K}$ and thus $L \simeq 12000\,L_\odot$, that the second overtone is found around 27 days together with linearly unstable higher-order modes. Such a drastic change of mass and luminosity within such a short time would be very unlikely. Thus, mode switching is virtually excluded.

We also may state that the pulsation of HD 56126 is very different from the one of RV Tauri stars. Indeed, the latter undergo a chaotic pulsation, very probably related to a 2:1 resonance between the fundamental mode (linearly unstable) and the first overtone, which both clearly appear as two large features in the Fourier spectrum (Tuchman et al. 1993, Fokin 1994, Buchler et al. 1996, Kolláth et al. 1998). On the contrary, for a star such as HD 56126, these two LNA modes are stable and, although their period ratio may reach 2, there is no significant Fourier component around 70–75 days. This originates from the higher temperature (at least 400 K more, with respect to RV Tau models assuming the same mass and gravity). In other terms, HD 56126 appears more evolved than post-AGB RV Tauri's.

4.2. Comparison with nonlinear models

Detailed nonlinear modelling of HD 56126 is beyond the scope of this paper, but we can compare our results with previous hydrodynamical calculations. There are indeed some puzzling facts to explain: the contrast between the large velocity amplitude and the very small photometric amplitude; the fact that the amplitude is so significant, while the period does not correspond to any pulsationally unstable mode and the linear growth rates of the only unstable overtones are (or, allowing for imperfect reflection, should be) relatively small.

For a detailed and rather pedagogical description of the atmospheric dynamics of stars (Pop. I and II Cepheids) not too different from the one we are interested in, it is worth reading Fokin & Gillet (1994) and Fokin et al. (1996). Concerning post-AGB stars more specifically, hydrodynamical calculations were performed by Aikawa (1991, 1993) and by Jeannin et al. (1996, 1997).

The latter attempted to model HD 56126, assuming however a somewhat shorter period. Several models with various fundamental parameters (some not too far from the above-mentioned most likely values, others with higher mass) exhibited an irregular pulsation with a small luminosity amplitude (~ 0.10–0.15 mag) but also a relatively large photospheric velocity amplitude ($\sim 15\,{\rm km\,s^{-1}}$), just like HD 56126. The first overtone was strongly excited, and also the second overtone in some models. A detailed investigation of the dynamics showed how the merger of successive shocks (generated at the compression and expansion phases) allowed the super-photospheric layers to reach a large velocity amplitude similar to the one derived by Lèbre et al. (1996) from Hα profiles (40–47 ${\rm km\,s^{-1}}$), which is 3 or 4 times larger than the photospheric velocity amplitude (see Fig. 3 above).

The indirect driving of a strong first-overtone pulsation despite the relatively small linear growth rates of the unstable modes may be explained by the mechanism described by Aikawa (1988): after maximum expansion of the star, in addition to the outgoing detached shock, a strong compression wave (called *w3* in Jeannin et al. 1996, 1997) is generated and propagates inwards. The resulting increase of density (and thus opacity) inside the ionization region enhances the driving effect of the κ-mechanism. Of course, the switching from the initial higher-order linear mode to the nonlinear first overtone should also help to increase the amplitude.

4.3. The structure of the atmosphere

4.3.1. A dynamical interaction of atmospheric layers?

We have seen in Sect. 2 and 3 that the Hydrogen Balmer line variations do not seem directly connected with the photospheric pulsation. Actually, the cores of these lines form within layers located above those where the metallic lines are generated. Then, if the pulsation amplitude is strong enough, these high atmospheric layers have not yet terminated their infalling motion when the deepest photospheric layers start a new upward motion. The interaction of these layers should produce a rather irregular motion. Moreover, since the mass transported by these layers is small, their dynamical effect onto the deeper (photospheric) ones is certainly weak. The motion of the upper layers is thus decoupled from the photosphere. If any kind of regularity (pseudo-period) appears besides the one corresponding to the input pulsation, it should be of the order of twice the free-fall time, i.e. 200–240 days according to the fundamental parameters that were derived above. Then, both the period of 272 days derived from Hα and its absence from the RV spectrum would be explained. Nevertheless, the successive shocks of different intensities arriving from photospheric layers can prevent this kind of regular motion of the high atmosphere.

4.3.2. A multi-shock structure?

Lèbre & Gillet (1991), using high resolution profiles of the sodium line at 5895.92 Å , showed that the motion of the high atmospheric layers of the pulsating RV Tauri star R Scuti is completely decoupled from the one of the photospheric region. For instance, they concluded that two shock waves are simultaneously present within the sodium layer. They qualitatively explained the multi-component structure of the line profile as the consequence of a doubling Schwarzschild phenomenon, i.e., the sodium layer is composed of a series of ascending and infalling sublayers. As RV Tauri stars are not very different from post-AGB stars, we may expect (subject to confirmation by a pulsa-

tion model) the atmospheric motion of HD 56126 to be as much complicated. Nevertheless, because our previous observations of the NaD2 line at 5889.95 Å (see paper I) do not show an obvious line doubling phenomenon, we expect that the atmosphere of HD 56126 does not present a well marked multi-component structure. However, this does not completely exclude that several shocks could be present at the same time within the hydrogen line formation region which is located closer from the photosphere. Each shock would have been formed during the two or three previous photospheric pulsation cycles. Thus, the multi-absorption structure observed within the core of the Hα profile (see Paper I, and Fig. 1 in this paper) would be due to several layers with different velocities.

4.3.3. An envelope emitting process?

Fadeyev & Fokin (1985) have shown that shock waves play a fundamental role in Pop. II Cepheids, by allowing a strong dissipation of the pulsational energy by radiation in the stellar atmosphere. In particular, this explains the existence of a limit cycle. The shock intensity becomes very large in giants and supergiants such as W Virginis, RV Tauri and other post-AGB stars. First, this means that the shocks become strongly radiative in the highest part of the atmosphere where hydrogen line cores are formed. Consequently, full understanding of the Hα emission profile requires non-LTE description of the radiative shock wake. Nevertheless, to date no such model is available, but important progresses are expected in the next few years (Fadeyev & Gillet 2000).

Due to the large intensity of these shocks in this part of the atmosphere, we must expect that an appreciable atmospheric extension takes place. Consequently, the atmosphere would be an expanding envelope with a complexe structure since sometimes several shells/shocks seem present (multi-absorption components within the Hα profile, see Paper I). This could perhaps explain why the shape of this line resembles to the characteristic *P-Cygni* or *inverse P-Cygni profiles* which means that the volume of the emitting region becomes enormous compared to that of the photosphere.

An unusual observationnal result of our survey is the almost permanent presence of the Hα emission (Fig. 1). This is not consistent with the classical pulsation picture because the pulsation period deduced from the metallic absorption lines, which are formed at the phostopheric level, is 36.8 days (Sect. 3). Nevertheless, it is perhaps possible to conciliate these two basic observationnal results in the framework of a pulsating/ballistic model in which the high atmosphere has an extended and decoupled multi-layer motion.

5. Conclusions

The main findings and conclusions of this work are the following:

– A new monitoring spectroscopic campaign of HD 56126 has permitted to confirm strong variations of the Hα line, and to show that variable emission wings also occur on Hβ. There is no clear periodicity or obvious timescale in these strange variations, in contrast to the metallic lines formed at the photospheric level, which follow the classical pulsation picture. Important changes can occur within an interval as short as 7 days. However, the position of the intensity minimum oscillates with a period of 272 days.
– From spectra of various origins, we have made a set of 89 daily averaged radial velocity data. A completely independent set of 87 V-band magnitudes has also been considered. These data have been analysed, using spectral and CLEAN-based methods. In spite of irregular sampling and seasonal gaps in the data set, a very clear main period of about 36.8 ± 0.2 days is found. The semi-amplitude of this component is found to be about $2.7\,\mathrm{km\,s^{-1}}$ (RV) and 0.02 magnitude (lightcurve), and leaves residual oscillations clearly above the noise level.
– Besides, only weak secondary periodicities are detected: they may have a physical meaning such as the irregularity of the stellar pulsation or the complexity of the resulting atmospheric dynamics. Their presence explains the above mentioned amplitude deficit. No strong secondary component can be found, especially none at $\sim 2P$, in contrast to RV Tauri stars.
– In order to understand the nature of the pulsation, linear nonadiabatic analysis has been performed as a first step. The only radial linear mode that fits the 36.8 period is the first overtone. LNA analysis puts constraints on the stellar fundamental parameters. Also taking into account the core mass-luminosity relation, we find: $\log g$ = 0.38–0.49, $M = 0.57$–$0.63\,M_\odot$, $T_{\rm eff}$ = 5700–6100 K and $L = 5250$–$8160\,L_\odot$ as the most likely values. Owing to its significantly higher temperature, HD 56126 is probably more evolved than post-AGB RV Tauri's.
– Confrontation with existing hydrodynamical models of similar stars has been performed. It follows that the irregular pulsation probably originates from the interaction between the photospheric dynamics and the one of the higher atmospheric layers. Shockwaves probably play a major role both in driving the pulsation (by supplementing the basic κ-mechanism) and limiting its amplitude. They must also be responsible for the very complicated motion of the outer layers (where the hydrogen line core forms), which is certainly not synchronous with the photospheric one, but develops its own, long timescale. More reliable nonlinear modelling requires the treatment of non-LTE radiative transfer in shocks, and is not yet available.
– One might expect that any study of the variability of HD 56126 based on radial velocity and light curves, with an 8 year-long dataset, be able to detect a component due to binary motion, if any, and to derive the orbital period (very likely years, and not a harmonic of the main pulsation period); or else, it should be able to rule out binarity. Many post-AGB and RV Tauri stars present evidences for binarity (van Winckel 1999). Concerning HD 56126, although its dust shell is already known to be asymmetric without any obvious explanation, binarity is very unlikely, but has not

yet been ruled out. Unfortunately, our spectroscopic and photometric data lead to ambiguous results; no long-term oscillation is reliably detected, but one observes the puzzling, statistically significant *coincidence* of a slight trend with a mismatch between the mean photospheric absorption and circumstellar emission velocities.

Acknowledgements. We warmly thank the visiting astronomers who performed observations with the 1.93 m O.H.P. telescope between October 1995 and April 1996, for their kind contribution to collecting spectroscopic data as regularly as possible. We are very grateful to Drs. E. Bakker and to Drs. G. Burki and C. Waelkens for providing us, respectively, with radial velocity measurements perfectly supplementing our own spectroscopic data, and with the Geneva photometry of HD 56126. Last, we are grateful to the anonymous referee for numerous remarks which contributed to improve this paper.

References

Aikawa T., 1988, ApSS 149, 149
Aikawa T., 1991, ApJ 374, 700
Aikawa T., 1993, MNRAS 262, 893
Baranne A., Queloz D., Mayor M. et al., 1996, A&AS 119, 373
Barthès D., Chenevez J., Mattei J., 1996, AJ 111, 2391
Bogaert, E., 1994, Ph.D. Thesis, Leuven University, Belgium
Bond, H.E., 1996, In: Livio M., Donahue M., Panagia N. (eds.), The Extragalactic Distance Scale, Cambridge Univ. Press, p. 224
Bond, H.E., 1997, In: Habing H.J., Lamers H. J. G. L. M. (eds.), Planetary nebulae, Kluwer, Dordrecht, p. 460
Boothroyd A.I., Sackmann I.J., 1988, ApJ 328, 641
Bressan A., Fagotto F., Bertelli G., Chiosi C., 1993, A&AS 100, 674
Buchler J.R., Kolláth Z., Serre T., Mattei J.A., 1996, ApJ 462, 489
Bujarrabal V., Alcolea J., Planesas P., 1992, A&A 257, 701
Castellani V., Chieffi A., Straniero O., 1992, ApJS 78, 517
Claret A., Giménez A., 1992, A&AS 96, 255
Cox J.P., Giuli R.T., 1968, Principles of Stellar Structure, Gordon and Breach Pub., New York
Fadeyev Yu.A., Gillet D., 2000, A&A 354, 349
Fadeyev, Yu. A., Fokin A.B., 1985, Ap&SS 111, 355
Fokin A.B., 1994, A&A 292, 133
Fokin A.B., Gillet D., 1994, A&A 290, 875
Fokin A.B., Gillet D., Breitfellner M.G., 1996, A&A 307, 503
Jeannin L., Fokin A.B., Gillet D., Baraffe I., 1996, A&A 314, L1
Jeannin L., Fokin A.B., Gillet D., Baraffe I., 1997, A&A 326, 203
Kaper L., Pasquini L., 1996, In: "CAT + CES Operating Manual", ESO Operating Manual, 3P6CAT-MAN-0633-0001.
Klochkova V.G., 1995, MNRAS 272, 710
Kolláth Z., Buchler J.R., Serre T., Mattei J.A., 1998, A&A 329, 147
Lèbre A., Gillet D., 1991, A&A 251, 549
Lèbre A., Mauron N., Gillet D., Barthès D., 1996. A&A 310, 923, (Paper I)
Parthasarathy M., Garcia-Lario P., Pottasch S.R., 1992, A&A 264, 159
Press W.H., Teukolsky S.A., Vetterling W.T., Flannery B.P., 1992, Numerical Recipes in Fortran, Cambridge Univ. Press
Scargle J.D., 1982, ApJ 263, 835
Schaller G., Schaerer D., Meynet G., Maeder A., 1992, A&AS 96, 269
Tuchman Y., Sack N., Barkat Z., 1978, ApJ 219, 183
Tuchman Y., Lèbre A., Mennessier M-O., Ya'ari A, 1993, A&A 271, 501
van Winckel H., 1999, In: Le Bertre T., Lèbre A., Waelkens C. (eds.), Asymptotic Giant Branch Stars (Proc. IAU Symp. 191, Montpellier, Aug. 1998), ASP, p 465